# *In situ* Measurement of Intense Optical Fields via Strong Field Ionization

Fan Xiao[1,2], Li Wang[1,2], Guangru Bai[1,2], Zhigang Zheng[1,2], Xu Sun[1,2], Tiefeng Ji[1,2], Yuchen Sun[3], Jiacan Wang[1,2], Xiaowei Wang[1,2*], and Zengxiu Zhao[1,2*]

[1]*Department of Physics, National University of Defense Technology, Changsha 410073, China*
[2]*Hunan Key Laboratory of Extreme Matter and Applications, National University of Defense Technology, Changsha 410073, China*
[3]*College of Systems Engineering, National University of Defense Technology, Changsha 410073, China*

(Received 28 January 2025; accepted manuscript online 12 March 2025)

This letter reports an all-optical measurement of laser electric field based on strong field ionization. By measuring the attosecond transient absorption spectra of krypton ions subjected to strong laser fields, we obtain the time-dependent effective valence-hole population, from which the driving laser waveform is retrieved with particle swarm optimization and genetic algorithm under strong-field approximation. Our *in situ* measurement approach underscores the capability of attosecond transient absorption spectroscopy (ATAS) to characterize intense laser fields accurately. This technique is pivotal for the analysis of electron dynamics in ATAS experiments, achieving a significant advancement in this field.

DOI: 10.1088/0256-307X/42/4/043701 CSTR: 32039.14.0256-307X.42.4.043701

Strong laser fields play important roles in the study of light–matter interactions. The temporal characterization of intense femtosecond pulses is vital for accurately investigating dynamical processes driven by their strong electric fields. Many techniques such as autocorrelation,[1,2] frequency-resolved optical gating (FROG),[3,4] spectral phase interferometry for direct electric field reconstruction (SPIDER),[5,6] dispersion scanning (D-scan),[7–9] and self-referenced spectral interferometry,[10,11] along with various improved variants,[12–15] have been proposed to obtain temporal profiles of ultra-short pulses through nonlinear processes. These methods are well-established, easy to implement, and widely applied due to their simplicity and effectiveness. However, the electric field waveforms cannot be directly accessed. Therefore, it is necessary to develop a direct measurement technique of strong laser electric fields.

To sample the electric field waveform of strong femtosecond pulses, ultrafast probes with pulse duration less than the oscillation period of carrier wave, i.e., attosecond pulses[16–19] are usually adopted. Attosecond streak camera,[20,21] which is the standard technique for the characterization of attosecond pulses, can also reconstruct the electric field of femtosecond streaking pulses simultaneously.[22–24] In addition to the attosecond pulses, attosecond electron dynamics in the three steps of high-order harmonic generation (HHG), i.e., the tunneling ionization, electron excursion, and radiative recombination,[25] can still serve the purpose of measuring the time-dependent field of a perturbative femtosecond pulses. One example is the petahertz optical oscilloscope,[26] in which the instantaneous electric field of femtosecond pulse to be measured is imprinted onto the deflection of HHG by asymmetrically altering the accumulated phase during electron excursion in a non-collinear geometry. Another example is the HHG cutoff, which is extremely sensitive to the driving field and can act as an indicator to retrieve the imperceptible electric field change.[27] In these two examples, the second and third steps in HHG are utilized respectively. The first step turns out to be powerful as well in light wave sampling, as demonstrated in the technique called tunneling ionization with a perturbation for the time-domain observation of an electric field (TIPTOE).[28–30] Moreover, it has been extended for long wavelength pulses via multiphoton excitation process other than strong field ionization.[31,32] In these measurements, however, the femtosecond pulses to be measured are kept weak so that they introduce only perturbation into the attosecond dynamics triggered by another much stronger probe pulse. In strong field experiments, the femtosecond near infrared (NIR) pulses are much intenser. Even if a weak replica of them can be measured, the actual waveform of intense pulses in the interaction region may be quite different due to nonlinear propagations in medium. It is necessary to detect the electric field of intense pulses right during the experiments driven by them.

In this letter, we demonstrate *in situ* measurements of intense optical fields based on strong field ionization during attosecond transient absorption spectroscopy (ATAS)[33] experiments. Time dependent effective hole populations (EHPs) in the strong field ionization are used to retrieve the pulse waveform. The connection between the EHPs and electric field of laser pulse is established in the framework of strong-field approximation (SFA).[34] And the retrieval is realized through the particle swarm optimization and genetic algorithm (PSOGA).[35–37] The waveform of

*Corresponding author. Email: xiaowei.wang@nudt.edu.cn; zhaozengxiu@nudt.edu.cn
© 2025 Chinese Physical Society and IOP Publishing Ltd. All rights, including for text and data mining, AI training, and similar technologies, are reserved.

6.6 fs ultrashort pulse is retrieved during the ionization of krypton atoms. The proposed scheme is an all-optical measurement technique, which has higher signal-to-noise level comparing to attosecond streak camera. Furthermore, the *in situ* measurements via ATAS are capable of reconstructing strong-field femtosecond pulse, which takes into account all the nonlinear effects during the laser interaction with gas target.

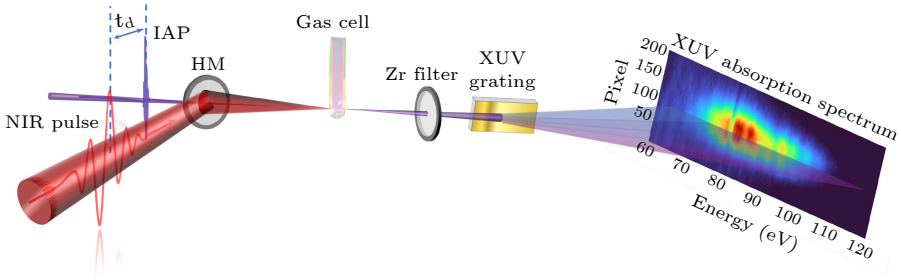


**Fig. 1.** Schematic drawing of the ATAS setup. A strong NIR pulse is used to ionize krypton atoms filled in a gas cell. The isolated attosecond pulse (IAP) is combined with the NIR pulse by a hole-drilled mirror (HM). After going through the cell, the NIR pulse is blocked by a Zr foil, while the IAP enters an extreme ultraviolet (XUV) spectrometer consisting of a flat field grating and micro-channel plates (MCP) detector.

The measurement was carried out with an ATAS setup shown in Fig. 1. A few-cycle NIR pulse centered at 750 nm was focused onto a gas cell filled with 60 mbar krypton. The pulse duration was estimated to be 5.1 fs through autocorrelation measurement. The laser peak intensity was determined to be $I = 3.3(\pm 0.3) \times 10^{14}\,\mathrm{W/cm^2}$ according to the cut-off energy law of HHG. Although it is a widely used method,[38–40] special care has to be taken to ensure good phase matching so that cut-off harmonics survive the propagation in the gas medium. To look into the strong field ionization dynamics, an IAP generated with double optical gating technique[41,42] was sent through the cell. The spectral range of the IAP was tuned to be 70–95 eV, which supported IAPs as short as 200 as taking into account the intrinsic atto-chirp and material dispersion. The relative delay between the two beams was stabilized (24 as time jitter) and scanned (141 as step size) with a delay line equipped with an active phase locking interferometer.[43] A home-built XUV spectrometer, which consists of a flat field grating and an assembly of MCPs and phosphor screens, was used to record the absorption spectra of IAP.

Krypton atoms get ionized at every peak of the laser electric field. And the krypton ions can be identified via the absorption line of IAPs corresponding to the transition from $4p_{3/2}^{-1}$ to $3d_{5/2}^{-1}$ (79.8 eV), as depicted in Fig. 2(a). The probability that an IAP photon to be absorbed is proportional to the number of krypton ions. The change of optical density, which is defined as $\Delta\mathrm{OD} = -\log(S_x^i/S_x^n)$[33,44] with $S_x^i$ and $S_x^n$ being the spectral intensity after absorption of $Kr^+$ (with NIR pulse) and neutral Kr (without NIR pulse), respectively. Although both $Kr^+$ and neutral Kr atoms coexist when NIR pulse is present, the absorption cross-section around 79.8 eV of $Kr^+$ is an order of magnitude larger than that of neutral Kr. Therefore, ΔOD is dominated by the absorption of $Kr^+$ with NIR pulse. As demonstrated in Ref. [44], ΔOD gives access to the real-time valence-hole population.

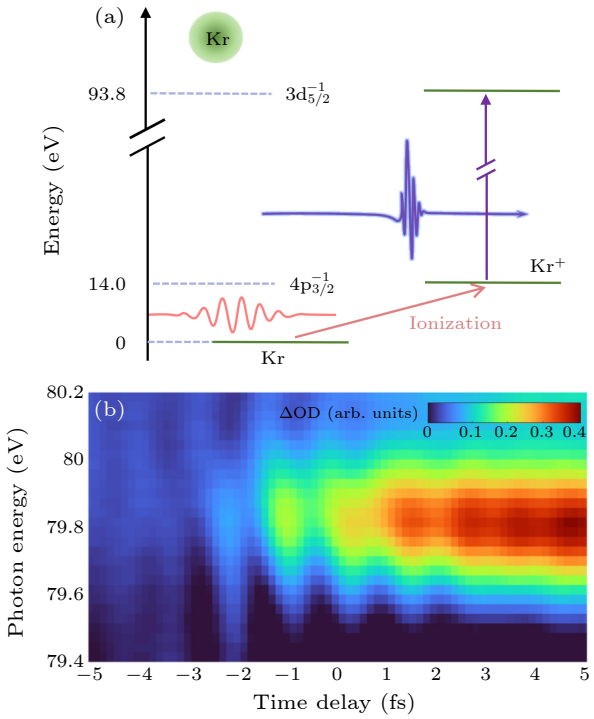


**Fig. 2.** (a) Diagram of relevant energy levels. Krypton ions are created in strong NIR fields, and are probed by the following IAPs through the transition of $4p_{3/2}^{-1}$ to $3d_{5/2}^{-1}$. (b) Measured change of optical density (ΔOD) in the vicinity of 79.8 eV as a function of time.

Figure 2(b) shows the experimentally measured ΔOD for different NIR-IAP delays. When IAP reaches the krypton atoms earlier than the NIR pulse, which is defined as negative delay in the figure, no krypton ions have been produced yet, so no noticeable change appears in the absorption spectra around 79.8 eV. By adjusting the time delay, IAP samples the real-time ion yield as the NIR laser field oscillates. According to the strong field ionization theory,[45] tunneling ionization dominates in the NIR laser fields with intensity corresponding to a Keldysh parameter of $\gamma \approx 0.6$. Tunneling occurs only around every peak of the laser field, when the atomic potential is sig-

nificantly changed. Therefore, ΔOD exhibits clearly half-cycle structures. Actually, a drop of absorption follows every increase, forming oscillations with period of half-laser-cycle, which has been reported before and termed as ionization "overshoot".[44] It is attributed to the transient ground-state polarization, acting as additional IAP photon absorber. Therefore, instead of instantaneous valence-hole population, ΔOD indicates the EHPs which are the the summation of the valence-holes and ground-state polarization.

However, it is not straightforward to extract EHP from ΔOD since the absorption feature undergoes line shape modifications under strong NIR fields, which can be described with the oscillating dipole model.[46] Following the same fitting procedure,[44] EHPs are obtained, as shown in Fig. 3(a). Although ATAS measures IAP spectra which are in essence the integration over a long time interval covering the duration of both NIR and IAP fields, it has been demonstrated that ATAS is capable of capturing the instantaneous strong field ionization dynamics on attosecond timescale.[44] Therefore, the EHP can be considered as instant responses of krypton atoms to strong NIR fields. It is thus possible to retrieve the NIR laser fields from the EHP if a proper theoretical model is developed to map the NIR field to EHP.

The map is established by solving the time-dependent Schrödinger equation (TDSE) under the single active electron approximation:

$$\mathrm{i}\frac{\partial}{\partial t}\Psi(t) = [H_0 + \boldsymbol{r}\cdot\boldsymbol{E}(t)]\Psi(t), \tag{1}$$

where $H_0$ is the field-free Hamiltonian, $\boldsymbol{E}(t)$ is the laser field, $\boldsymbol{r}$ is the position operator, and $\Psi(t)$ is the time-dependent wave function including both the neutral ground state $\Psi_\mathrm{g}$ and continuum state $\Psi_\mathrm{c}$:

$$\Psi(t) = a_\mathrm{g}\Psi_\mathrm{g} + \int a_\mathrm{c}(\boldsymbol{p}, t)\Psi_\mathrm{c}(\boldsymbol{p})\mathrm{e}^{-\mathrm{i}S(\boldsymbol{p}, t)}\mathrm{d}\boldsymbol{p}, \tag{2}$$

with $a_\mathrm{g}$ being the probability amplitude of the neutral ground state, $a_\mathrm{c}(\boldsymbol{p}, t)$ the probability amplitude of the continuum state at the momentum $\boldsymbol{p}$, and $S(\boldsymbol{p}, t)$ the action.[47] The probability amplitude of the continuum state can be simplified using SFA as

$$a_\mathrm{c}(\boldsymbol{p}, t) = -\mathrm{i}\int_{-\infty}^{t}\langle\Psi_\mathrm{c}|\boldsymbol{r}\cdot\boldsymbol{E}(t')|\Psi_\mathrm{g}\rangle\mathrm{e}^{-\mathrm{i}S(\boldsymbol{p}, t')}\mathrm{d}t'. \tag{3}$$

Then the effective valence-hole population $\rho^\mathrm{eff}(t)$ can be calculated as

$$\rho^\mathrm{eff}(t) = \int |a_\mathrm{c}(\boldsymbol{p}, t)|^2\mathrm{d}\boldsymbol{p}. \tag{4}$$

In the calculation, the instantaneous SFA ionization probability is obtained through the integration over the laser-dressed continuum states, explicitly incorporating

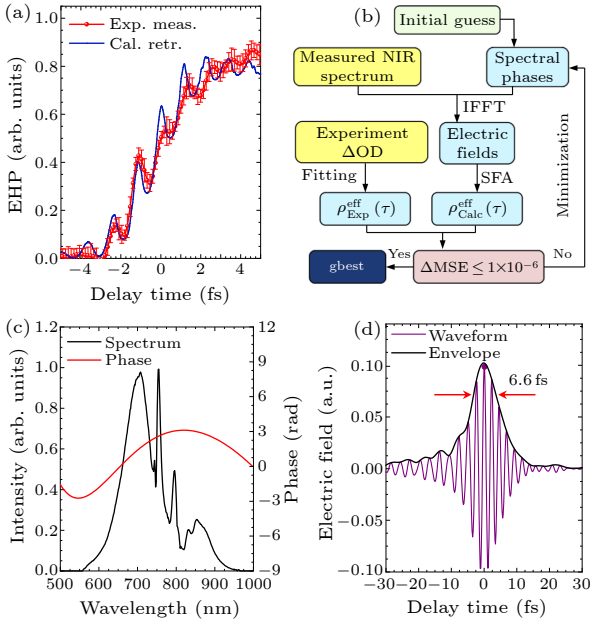


**Fig. 3.** The retrieval of strong NIR laser fields. (a) The comparison between experimentally measured EHP (dotted line) with retrieved EHP (solid line). (b) The flow chart of PSOGA optimization. The algorithm starts with a group of initial randomly guessed particles. Each particle corresponds to a laser field with which $\rho^\mathrm{eff}_\mathrm{Calc}$ is calculated and compared with EHP $\rho^\mathrm{eff}_\mathrm{Exp}$ to obtain evaluation errors. The particles are updated through minimization process and convergence will be eventually reached as the iteration goes on. (c) the measured spectral profile (black curve) and retrieved phases (red curve). (d) the retrieved electric field (purple curve) and its amplitude (black curve). The full width at half maximum (FWHM) of the pulse is 6.6 fs.

electron-hole coherence effects induced by the strong-field ionization. This quantum coherence manifests as sub-cycle modulations and reproduces the experimental observed ionization "overshoot" in the time-dependent ionization probability. Although not as accurate as solving TDSE with Coulomb potential included, SFA can achieve decent results[33] more quickly. However, SFA is not capable of predicting the total ionization probability quantitatively,[48] leading to an arbitrary scaling factor of the peak laser intensity. In the measurements, the peak laser intensity is pre-calibrated via HHG cut-off energy. With the above procedure, time-dependent EHPs can be obtained for any given laser field. The remaining task is to find the right NIR field that matches the experimentally measured EHP.

To simplify the problem, we measure the NIR spectral profile beforehand, so that we only need to retrieve the spectral phases. The spectral phases are further expanded as Fourier series with harmonics up to 8th order, i.e., the NIR field is represented by 18 parameters (17 coefficients and the central wavelength). Note that the peak intensity is known as well. The retrieval is then converted to an optimization problem for 18 variables. There are lots of optimization algorithms that would work for complex multivariate optimization problems, such as genetic algorithm (GA), simulated annealing algorithm, particle swarm optimization (PSO), and neural networks algorithms. We

adopted PSOGA here, which is a hybrid optimization algorithm that combines PSO and GA. Every set of variables is called a particle in the algorithm. The flow chart of the retrieval is depicted in Fig. 3(b).

The retrieval starts with a group of initial randomly guessed particles, then NIR fields are obtained via inverse Fourier transform from measured spectral profile and guessed phases. Since the electric field can be shaped via the spectral phases, the large set of random phases result in all kinds of complex pulse shapes including double pulses, long pulses, and satellite pulses, which ensures the robustness of the retrieval. The NIR fields are then sent to the SFA model to calculate time-dependent EHP $\rho^{\rm eff}_{\rm Calc}$ with which the experimental measured EHP $\rho^{\rm eff}_{\rm Exp}$ is compared to obtain evaluation errors. The minimization is done via genetic evolution and PSO updating based on personal best (pbest) and global best (gbest). As the iteration goes on, the gbest converges. The iteration stops when the minimum mean squared error (MSE) does not reduce (by $1\times10^{-6}$) anymore in the successive iterations, and the final MSE of the converged solution was $2.6\times10^{-3}$ which suggests a good convergence.

The retrieved EHP is shown as the solid line in Fig. 3(a), which matches the experimental measurements qualitatively. The retrieved phases along with the measured spectral profile of the NIR pulse are shown in Fig. 3(c) as red and black curves, respectively. There exist high-order dispersions in the spectral phases, which yields a non-symmetric temporal profile shown in Fig. 3(d). The maximum field intensity is $4.97\times10^{10}$ V/m, which is determined by the pre-calibrated peak intensity. And the pulse duration, i.e., FWHM of $|E(t)|^2$ is 6.6 fs. Note that the algorithm cannot determine the sign of the electric field, namely, the carrier envelope phase can be changed by integer multiples of $\pi$.

To verify the retrieval, the fringe-resolved autocorrelation (FRAC) trace of a weak replica (7‰) of the strong NIR field is measured, as shown in Fig. 4 (dotted line).

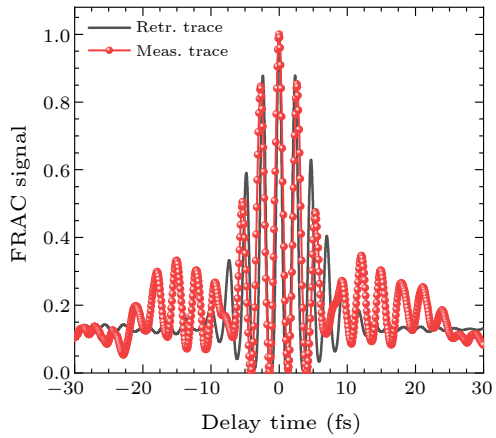


**Fig. 4.** The comparison between measured FRAC trace (dotted line) and retrieved FRAC trace (solid line). In the central part where the intensity part of the two autocorrelation beam overlaps, the retrieval agrees well with the measurement. The two additional interference structures on both sides, which may be attributed to small satellite pulses, are absent in the retrieved trace. The discrepancy is rooted in the measurement principle, i.e., strong field ionization.

The trace suggests a pulse duration of 5.1 fs, which is only a referential estimation. It is more meaningful to compare the measured FRAC trace with the calculated trace based on the retrieved electric field, as shown as the black solid line in Fig. 4. The two traces agree well with each other in the central part while the electric field is strong. Whereas in both sides of the central interference of the measured trace, there are two additional interference structures which may be attributed to small satellite pulses. And the retrieval fails to reconstruct the weak satellite pulses. It is because that the retrieval is accomplished with strong field ionization which nonlinearly depends on the pulse intensity, therefore, the weak edges are subject to arbitrary alteration as long as they are weak enough to avoid ionization. Regarding to the discrepancy, the pulse intensity difference could be responsible, and the limitation of the SFA might be another factor. The proposed method works only for the measurement of intense optical fields, however, it has the ability to *in situ* sample the femtosecond electric field during the experiments, which detects all the waveform distortions in the interaction process.

In conclusion, the electric field of few-cycle intense femtosecond pulses is successfully retrieved through strong field ionization of krypton atoms in ATAS experiments. The real-time evolution of the EHP was extracted from the $\Delta$OD and utilized to reconstruct the NIR laser field with PSOGA. The accuracy of the retrieved main pulse was confirmed by comparison with autocorrelation measurements. This approach serves as a valuable complement to the existing electric field sampling techniques and holds significant potential for advancing the study of atomic and molecular dynamics in strong laser fields.

*Acknowledgements.* This work was supported by the National Natural Science Foundation of China (Grant Nos. 12234020, 12450403, and 12374263).

# References

[1] Fork R L and Beisser F A 1978 *Appl. Opt.* **17** 3534
[2] Wasylczyk P 2001 *Rev. Sci. Instrum.* **72** 2221
[3] Kane D and Trebino R 1993 *IEEE J. Quantum Electron.* **29** 571
[4] Trebino R, DeLong K W, Fittinghoff D N, Sweetser J N, Krumbügel M A, Richman B A, and Kane D J 1997 *Rev. Sci. Instrum.* **68** 3277
[5] Iaconis C and Walmsley I A 1998 *Opt. Lett.* **23** 792
[6] Wemans J, Figueira G, Lopes N, and Cardoso L 2006 *Opt. Lett.* **31** 2217
[7] Miranda M, Fordell T, Arnold C, L'Huillier A, and Crespo H 2011 *Opt. Express* **20** 688
[8] Miranda M, Arnold C L, Fordell T, Silva F, Alonso B, Weigand R, L'Huillier A, and Crespo H 2012 *Opt. Express* **20** 18732
[9] Fabris D, Holgado W, Silva F, Witting T, Tisch J W G, and Crespo H 2015 *Opt. Express* **23** 32803
[10] Chung J H and Weiner A 2001 *IEEE J. Sel. Top. Quantum Electron.* **7** 656
[11] Yamane K, Kito T, Morita R, and Yamashita M 2004 *Opt. Express* **12** 2762
[12] Kosik E M, Radunsky A S, Walmsley I A, and Dorrer C 2005 *Opt. Lett.* **30** 326
[13] Birge J R, Ell R, and Kärtner F X 2006 *Opt. Lett.* **31** 2063

[14] Birge J R, Crespo H M, and Kärtner F X 2010 *J. Opt. Soc. Am. B* **27** 1165
[15] Witting T, Frank F, Okell W A, Arrell C A, Marangos J P, and Tisch J W G 2012 *J. Phys. B: At. Mol. Opt. Phys.* **45** 074014
[16] Gaumnitz T, Jain A, Pertot Y, Huppert M, Jordan I, Ardana-Lamas F, and Wörner H J 2017 *Opt. Express* **25** 27506
[17] Li J, Ren X, Yin Y, Zhao K, Chew A, Cheng Y, Cunningham E, Wang Y, Hu S, Wu Y, Chini M, and Chang Z 2017 *Nat. Commun.* **8** 186
[18] Wang X, Wang L, Xiao F, Zhang D, Lü Z, Yuan J, and Zhao Z 2020 *Chin. Phys. Lett.* **37** 023201
[19] Wang X, Xiao F, Wang J, Wang L, Zhang B, Liu J, Zhao J, and Zhao Z 2024 *Ultrafast Sci.* **4** 0080
[20] Itatani J, Quéré F, Yudin G L, Ivanov M Y, Krausz F, and Corkum P B 2002 *Phys. Rev. Lett.* **88** 173903
[21] Mairesse Y and Quéré F 2005 *Phys. Rev. A* **71** 011401
[22] Goulielmakis E, Uiberacker M, Kienberger R, Baltuska A, Yakovlev V, Scrinzi A, Westerwalbesloh T, Kleineberg U, Heinzmann U, Drescher M, and Krausz F 2004 *Science* **305** 1267
[23] Wirth A, Hassan M T, Grguraš I, Gagnon J, Moulet A, Luu T T, Pabst S, Santra R, Alahmed Z A, Azzeer A M, Yakovlev V S, Pervak V, Krausz F, and Goulielmakis E 2011 *Science* **334** 195
[24] Zhong S, Teng H, Zhu X, Gao Y, Wang K, Wang X, Wang Y, Yu S, Zhao K, and Wei Z 2023 *Chin. Opt. Lett.* **21** 113201
[25] Corkum P B 1993 *Phys. Rev. Lett.* **71** 1994
[26] Kim K T, Zhang C, Shiner A D, Schmidt B E, Légaré F, Villeneuve D M, and Corkum P B 2013 *Nat. Photon.* **7** 958
[27] Wyatt A S, Witting T, Schiavi A, Fabris D, Matia-Hernando P, Walmsley I A, Marangos J P, and Tisch J W G 2016 *Optica* **3** 303
[28] Park S B, Kim K, Cho W, Hwang S I, Ivanov I, Nam C H, and Kim K T 2018 *Optica* **5** 402
[29] Cho W, Hwang S I, Nam C H, Bionta M R, Lassonde P, Schmidt B E, Ibrahim H, Légaré F, and Kim K T 2019 *Sci. Rep.* **9** 16067
[30] Cho W, Shin J U, and Kim K T 2021 *Sci. Rep.* **11** 13014
[31] Liu Y, Gholam-Mirzaei S, Beetar J E, Nesper J, Yousif A, Nrisimhamurty M, and Chini M 2021 *Photon. Res.* **9** 929
[32] Liu Y, Beetar J E, Nesper J, Gholam-Mirzaei S, and Chini M 2022 *Nat. Photon.* **16** 109
[33] Wang L, Bai G, Wang X, Zhao J, Gao C, Wang J, Xiao F, Tao W, Song P, Qiu Q, Liu J, and Zhao Z 2024 *Nat. Commun.* **15** 2705
[34] Zhao J, Liu J, Wang X, Yuan J, and Zhao Z 2022 *Chin. Phys. Lett.* **39** 123201
[35] Garg H 2016 *Appl. Math. Comput.* **274** 292
[36] Zhu Q B, Zhang Z X, Tong L Y, Li T J, Geng M M, Xu W C, Zhang Z R, and Luo Z C 2023 *Opt. Express* **31** 40498
[37] Sabouri A and Perez-Martinez C S 2024 *Ultramicroscopy* **266** 114024
[38] Cirmi G, Lai C J, Granados E, Huang S W, Sell A, Hong K H, Moses J, Keathley P, and Kärtner F X 2012 *J. Phys. B: At. Mol. Opt. Phys.* **45** 205601
[39] Luu T T, Yin Z, Jain A, Gaumnitz T, Pertot Y, Ma J, and Wörner H J 2018 *Nat. Commun.* **9** 3723
[40] Mondal A, Neufeld O, Yin Z, Nourbakhsh Z, Svoboda V, Rubio A, Tancogne-Dejean N, and Wörner H J 2023 *Nat. Phys.* **19** 1813
[41] Chang Z 2007 *Phys. Rev. A* **76** 051403
[42] Feng X, Gilbertson S, Mashiko H, Wang H, Khan S D, Chini M, Wu Y, Zhao K, and Chang Z 2009 *Phys. Rev. Lett.* **103** 183901
[43] Chini M, Mashiko H, Wang H, Chen S, Yun C, Scott S, Gilbertson S, and Chang Z 2009 *Opt. Express* **17** 21459
[44] Sabbar M, Timmers H, Chen Y J, Pymer A K, Loh Z H, Sayres S, Pabst S, Santra R, and Leone S R 2017 *Nat. Phys.* **13** 472
[45] Keldysh L V 1965 *J. Exp. Theor. Phys.* **20** 1307
[46] Pabst S, Sytcheva A, Moulet A, Wirth A, Goulielmakis E, and Santra R 2012 *Phys. Rev. A* **86** 063411
[47] Lewenstein M, Balcou P, Ivanov M Y, L'Huillier A, and Corkum P B 1994 *Phys. Rev. A* **49** 2117
[48] Popruzhenko S V 2014 *J. Phys. B: At. Mol. Opt. Phys.* **47** 204001